

# A foundation for exact binarized morphological neural networks

Theodore Aouad

Universite Paris-Saclay, CentraleSupélec, Inria, CVN  
3 rue Joliot Curie, Gif-sur-Yvette, France  
theodore.aouad@centralesupelec.fr

Hugues Talbot

Universite Paris-Saclay, CentraleSupélec, Inria, CVN  
3 rue Joliot Curie, Gif-sur-Yvette, France  
hugues.talbot@centralesupelec.fr

## Abstract

*Training and running deep neural networks (NNs) often demands a lot of computation and energy-intensive specialized hardware (e.g. GPU, TPU...). One way to reduce the computation and power cost is to use binary weight NNs, but these are hard to train because the sign function has a non-smooth gradient. We present a model based on Mathematical Morphology (MM), which can binarize ConvNets without losing performance under certain conditions, but these conditions may not be easy to satisfy in real-world scenarios. To solve this, we propose two new approximation methods and develop a robust theoretical framework for ConvNets binarization using MM. We propose as well regularization losses to improve the optimization. We empirically show that our model can learn a complex morphological network, and explore its performance on a classification task.*

## 1. Introduction

Binary weight neural networks (BWNNs) are attractive because they can provide powerful machine learning solutions with much less storage, computation, and energy consumption than conventional networks [21]. Several methods, such as BinaryConnect [5], DoReFa-Net [27], and XNOR-Net [21], have shown good to excellent results in a variety of applications. These networks usually use the sign function to binarize the weights in the forward pass. They must use a special gradient function, like the Straight-Through Estimator (STE) [3], to overcome the zero gradient problem of the sign function during the backward pass. However, this approach lacks a solid theoretical basis, suggesting the need for a different approach. Some methods avoid using the STE by first training a floating-point neural

network and then binarizing it afterwards [12, 8]. However, this approach may lead to approximate binarization and a drop in performance. In this paper, we present a new approach that uses the concepts of Mathematical Morphology (MM) [23] to overcome the drawbacks of existing methods. MM, based on modern set theory and complete lattices, offers a non-linear mathematical framework for image processing. Its basic operators, erosion and dilation, are equivalent to thresholded convolutions [14], creating a link between MM and deep learning. Combining these fields can improve the efficiency and results of morphological operations while enhancing our knowledge of deep learning [1]. Recent works on morphological neural networks have explored learning operators and structuring elements using various approaches, such as the max-plus definition [19, 6] and differentiable approximations [24, 18, 9]. However, these methods primarily focus on learning gray-scale MM operators and have not focused on NN binarization.

The Binary Morphological Neural Network (BiMoNN) [2] proposed a well-defined mathematical method that can binarize NN weights without losing performance under certain conditions. However, it is limited to binary inputs and can learn only one filter per layer, limiting the design of modern architectures. In this paper, we improve the BiMoNN framework to overcome these limitations and introduce a new model that can learn any sequence of morphological operators while achieving complete binarization in all cases. We also introduce novel regularization techniques to encourage our model to become morphological. By combining MM concepts with deep learning, our work establishes the basis for a more robust and theoretically sound framework for NN binarization. Our contributions in this work are as follows:

- In §2, we refine the BiMoNN theoretical framework and generalize it to any kind of gray-scale / RGB inputs. We

introduce two new layers analogous to the dense and convolutional layers, enabling the transposition of modern architectures.

- In §3, we present a well-defined mathematical binarization method based on MM that works seamlessly with standard frameworks and tools. We also propose two new approximate binarization techniques to deal with the cases where exact binarization is not possible.
- In §4, we introduce three applicable regularization losses, and a fourth one that is only theoretical due to its long computation time.
- In §5, we evaluate the capacity of the binarized BiMoNN to learn complex morphological pipelines without performance loss. Additionally, we investigate its behavior on the MNIST [16] classification task, and the behavior of the introduced regularization techniques.

Our code is publicly available at <https://github.com/TheodoreAouad/LBQNN2023>.

## 2. General Binary Morphological Neural Network

We build on the BiMoNN framework [2] and propose a new Binary Structuring Element (BiSE) neuron. We show how it is morphologically equivalent to binary images by using the notion of almost binary images. We also propose the BiSE Layer (BiSEL) that can learn multiple filters per layer, which is similar to a convolutional layer; and the DenseLUI, a dense layer that can be binarized. In §2.1 and §2.2, we consider binary inputs only. We generalize to any types of inputs in §2.3.

### 2.1. Binary Structuring Element neuron

Let  $D$  be the dimension of the image (usually  $D = 2$  or  $3$ ). We denote  $\Omega_I \subset \mathbb{Z}^D$  the support of the images, and  $\Omega$  the support of the weights kernel. For the remainder of the paper, we assume  $S \subset \Omega$  and  $S \neq \emptyset$ . For a set  $X \subset \mathbb{Z}^D$ , we denote its indicator function  $\mathbb{1}_X : \mathbb{Z}^D \mapsto \mathbb{R}$  such that  $\mathbb{1}_X(i) = 1$  if  $i \in X$ , else  $\mathbb{1}_X(i) = 0$ . We denote the set of its subsets  $\mathcal{P}(X)$ . We denote the convolution by  $\otimes$ . We denote  $[\cdot]_+ := \max(\cdot, 0)$  and  $[\cdot]_- := \min(\cdot, 0)$ .

**Definition 2.1** (BiSE neuron). Let  $(W, B)$  be a set of reparametrization functions and  $(\omega, \beta, p)$  a set of learnable parameters. Let  $\xi$  be a smooth threshold activation (e.g. normalized tanh:  $\frac{1}{2} \tanh(\cdot) + \frac{1}{2}$ ). Then the *Binary Structuring Element neuron* (BiSE) is:

$$\chi : \mathbf{x} \in [0, 1]^{\Omega_I} \mapsto \xi \left( p \left[ \mathbf{x} \otimes W(\omega) - B(\beta) \right] \right) \in [0, 1]^{\Omega_I} \quad (1)$$

The reparametrization functions  $(W, B)$  are hyperparameters. The BiSE neuron is a convolution operator with weights and biases that are reparametrized (see §2.4), a

smooth threshold activation and a scaling factor  $p$  that can invert the output if negative. We introduce the following *almost binary* image representation, to handle images that are not exactly binary and to be able to apply gradient descent optimization.

**Definition 2.2** (Almost Binary Image). The set of almost binary images of parameter  $\delta$  is denoted  $\mathcal{I}(\delta)$ . We say an image  $\mathbf{I} \in [0, 1]^{\Omega_I}$  is *almost binary* and define  $X_{\mathbf{I}}$  its *associated binary image* if:

$$\exists \delta \in \left] 0, \frac{1}{2} \right], \mathbf{I}(\Omega_I) \cap \left] \frac{1}{2} - \delta, \frac{1}{2} + \delta \right[ = \emptyset \quad (2)$$

$$X_{\mathbf{I}} := \left( \mathbf{I} > \frac{1}{2} \right) \quad (3)$$

### 2.2. Morphological Equivalence

We now express the conditions under which a BiSE neuron can be seen as a morphological operator.

**Theorem 2.3** (Dilation - Erosion Equivalence). *For a given structuring element (SE)  $S \subset \Omega$ , and an almost binary parameter  $\delta \in ]0, \frac{1}{2}]$ , a set of reparametrized weights  $\mathbf{W} \in \mathbb{R}^{\Omega}$  and bias  $b \in \mathbb{R}$ , we define:*

$$L_{\oplus}(\mathbf{W}, S) := \sum_{k \in \Omega \setminus S} [\mathbf{W}_k]_+ + \left( \frac{1}{2} - \delta \right) \sum_{k \in S} [\mathbf{W}_k]_+ \quad (4)$$

$$U_{\oplus}(\mathbf{W}, S) := \left( \frac{1}{2} + \delta \right) \min_{k \in S} \mathbf{W}_k + \sum_{k \in \Omega} [\mathbf{W}_k]_- \quad (5)$$

$$U_{\ominus}(\mathbf{W}, S) := \sum_{k \in \Omega} \mathbf{W}_k - L_{\oplus}(\mathbf{W}, S) \quad (6)$$

$$(7)$$

$$L_{\ominus}(\mathbf{W}, S) := \sum_{k \in \Omega} \mathbf{W}_k - U_{\oplus}(\mathbf{W}, S) \quad (8)$$

Let  $\psi \in \{\oplus, \ominus\}$  be a dilation or erosion. Then:

$$\forall I \in \mathcal{I}(\delta), \psi_S \left( \mathbf{I} > \frac{1}{2} \right) = \left( \mathbf{I} \otimes W > b \right) \\ \Leftrightarrow L_{\psi}(\mathbf{W}, S) \leq b < U_{\psi}(\mathbf{W}, S) \quad (9)$$

In this case,  $\forall s \in S, \mathbf{W}_s \geq 0$  and  $b \geq 0$  and we say that a BiSE  $\chi$  with weights  $W(\omega) = \mathbf{W}$  and  $B(\beta) = b$  is **activated**. If  $\psi = \oplus$ , then  $B(\beta) \leq \frac{1}{2} \sum_{k \in \Omega} W(\omega)_k$ . If  $\psi = \ominus$ , then  $B(\beta) \geq \frac{1}{2} \sum_{k \in \Omega} W(\omega)_k$ .

For any almost binary image  $\mathbf{I} \in \mathcal{I}(\delta)$ ,  $\chi(\mathbf{I}) \in \mathcal{I}(\delta_{out})$  is almost binary with known parameter  $\delta_{out}$ . Finally

$$\forall I \in \mathcal{I}(\delta), \left( \chi(\mathbf{I}) > \frac{1}{2} \right) = \psi_S \left( \mathbf{I} > \frac{1}{2} \right) \quad (10)$$

$$\begin{array}{ccc} \mathbf{I} & \xrightarrow{\chi} & \chi(\mathbf{I}) \\ \downarrow \cdot > \frac{1}{2} & & \downarrow \cdot > \frac{1}{2} \\ X_{\mathbf{I}} & \xrightarrow{\psi_S} & X_{\chi(\mathbf{I})} \end{array}$$

This theorem states that if a BiSE is activated, it transforms an almost binary inputs into an almost binary outputs with known  $\delta_{out}$ . Moreover, if we threshold the input and output with respect to  $\frac{1}{2}$ , it is equivalent to applying the corresponding morphological operation, exhibiting an almost commutativity property between thresholding and convolution. Further, equation (10) shows that if a BiSE is activated for operation  $\psi$ , performing the BiSE operation in  $\mathcal{I}(\delta)$  is equivalent to performing the binary morphological operation  $\psi$  in the binary space  $\mathcal{P}(S)$ . This presents a natural framework for binarization (see §3).

### 2.3. Binary Morphological Neural Network

Our objective is to build a binarizable neural network. We now define binarizable neural layers based on the BiSE neuron. By combining these layers, we can create flexible architectures tailored to the desired task.

As mentioned earlier, the BiSE neuron resembles a convolution operation. However, a single convolution is insufficient to create a morphological layer. In this context, we explain how we handle multiple channels. We observe that the BiSE neuron can be used to define a layer that learns the intersection or union of multiple binary images  $\mathbf{x}_1, \dots, \mathbf{x}_n \in \mathcal{I}(\delta)$ . For example, their union can be expressed as the dilation of the 3D image  $\mathbf{x} := (\mathbf{x}_1, \dots, \mathbf{x}_n) \in \mathcal{I}(\delta) \subset ([0, 1]^{\Omega_I})^n$  with a tubular SE applied solely across the dimension of depth. Therefore, we define the Layer Union Intersection (LUI) as a special case of the BiSE layer, with weights restricted to deep-wise shape. It is analogous to a  $1 \times 1$  convolution unit. A LUI layer can learn any intersection or union of any number of almost binary inputs. By combining BiSE neurons and LUI layers, we can learn morphological operators and aggregate them as unions or intersections.

**Definition 2.4** (BiSEL). A BiSEL (BiSE Layer) is the combination of multiple BiSE and multiple LUI. Let  $(\chi_{n,k})_{n,k}$  be  $N * K$  BiSE and  $(LUI_k)_k$  be  $K$  LUI. Then we define a BiSEL as:

$$\phi : \mathbf{x} \in ([0, 1]^{\Omega_I})^N \mapsto \left( LUI_k \left[ (\chi_{n,k}(\mathbf{x}_n))_n \right] \right)_k \quad (11)$$

The BiSEL mimics a convolutional layer. In conventional ConvNets, to process multiple input channels, a separate filter is applied to each channel, and their outputs are summed to create one output channel. In the case of BiSEL, instead of summing the results of each filter, we perform a union or intersection operation (see Figure 1).

**DenseLUI** the LUI layer is similar to a  $1 \times 1$  convolution, which is equivalent to a fully connected layer. Given an input vector  $\mathbf{x} \in \mathbb{R}^n$ , we can apply the LUI layer to the

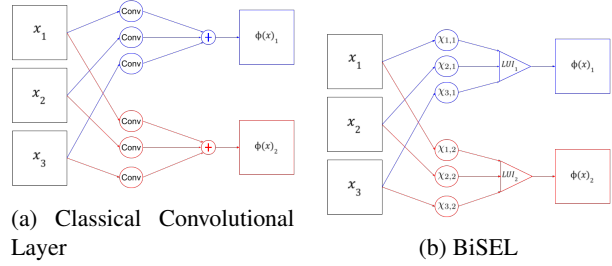


Figure 1: BiSEL vs Conv Layer. Input  $\mathbf{x}$  with 3 channels. Output  $\phi(\mathbf{x})$  with 2 channels.

reshaped input  $\hat{\mathbf{x}} \in \mathbb{R}^{n \times 1 \times 1}$  treating it as a 2D image with width and length of 1 and  $n$  channels, respectively. Therefore, we can utilize the BiSEL to create binarizable fully connected layers.

**Gray-Scale / RGB Inputs** Up until now, all inputs were assumed binary. We extend these definitions to gray-scale and RGB images. The main idea is to separate an input channel  $\mathbf{I}_c \in \mathbb{R}^{\Omega_I}$  into its set of upper level-sets to come back to binary inputs:

$$\{(\mathbf{I}_c \geq \tau) \mid \tau \in \mathbb{R}\} \quad (12)$$

Considering all possible values of  $\tau$  from a continuous image would result in an excessive number of level-sets to process. Alternatively, we can define a finite set of values for  $\tau$  in advance. Subsequently, each channel of an image  $\mathbf{I} \in \mathbb{R}^{c \times w \times l}$  is separated into its corresponding level-sets, and these level-sets are provided as additional channels. If we have  $N$  values for level-set, the resulting input is a binary image  $\mathbf{I}_{\mathbb{B}} \in \{0, 1\}^{(N \cdot c) \times w \times l}$ .



Figure 2: Gray to level-set for 5 different values, generating 5 input channels.

We have introduced two types of binarizable layers: the DenseLUI, which is similar to a fully connected layer, and the BiSEL, which resembles a convolutional layer. By combining these layers, we can create a Binary Morphological Neural Network (BiMoNN), which encompasses various architectures suited for different tasks.

### 2.4. Training considerations

The BiMoNN ( $\Gamma_{\mathbb{R}}$ ) is fully differentiable. If  $\mathcal{L}$  is a differentiable loss function, given a dataset of  $N$  labeled images  $\{(\mathbf{x}_i, \mathbf{y}_i)\}$ , we minimize the error  $\frac{1}{N} \sum_{i=1}^N \mathcal{L}(\Gamma_{\mathbb{R}}(\mathbf{x}_i), \mathbf{y}_i)$  using a gradient descent algorithm (like Adam [13]). The

gradients are computed with the backpropagation algorithm [22]. The binarization scheme, which is defined in the next section, is applied post-training or during training to measure the model’s evolution.

To facilitate the convergence of our networks towards morphological operators, certain constraints are beneficial. In order to avoid dealing with a multitude of constraints, we reparametrize some variables to ensure that the constraints are always satisfied. We introduce two reparametrization functions for the weights, and three for the bias.

**Positivity** Our objective is to reach the set of activable weights and bias. Theorem 2.3 indicates that we only have to look at positive parameters. We can enforce them to be positive by setting  $W$  and  $B$  as the softplus function:

$$B_{pos}(\cdot) = W_{pos}(\cdot) := f^+(\cdot) := \log(1 + \exp(\cdot)) \quad (13)$$

**Dual reparametrization** For the weights, we introduce the *dual* reparametrization as follows:

$$W_{dual}(\omega) := \frac{K \cdot f^+(\omega)}{\sum_{W(\omega)} w} \quad (14)$$

with  $K := 2 \cdot \xi^{-1}(0.95)$ . We can show that this dual reparametrization ensures that the training process is similar for both erosion and dilation.

Other reparametrization for the bias can be defined to keep it into coherent range values. If the bias is smaller than  $\min(W)$ , then  $\forall X \subset \Omega, \chi(\mathbb{1}_X) < 0.5$ : no values will be close to 1. On the other side, if the bias is higher than  $\sum_W w$ , then  $\chi(\mathbb{1}_X) > 0.5$ . Therefore, we want  $\min(W) < B < \sum_W w$ . Let  $\{W_1 < \dots < W_K\}$  be the ordered values taken by the weights  $W$ . The previous inequality is ensured if  $B$  belongs to the closed convex set  $C_b := [\frac{W_1+W_2}{2}, \sum_W w - \frac{W_1}{2}] = [l_c(W), u_c(W)]$ . There are two ways of ensuring that  $B \in C_b$ .

**Projected** First, we can project the bias after the gradient iteration: this comes down to a projected gradient algorithm. We call this approach ”Projected” reparametrization. We apply  $B_p(\beta) := f^+(\beta)$ , and we project  $B_p(\beta)$  onto  $C_b$  after the gradient update iteration.

**Projected Reparam** The second way is to redefine  $B$  before the end of the iteration, instead of after. We call this approach ”Projected Reparam” reparametrization:

$$B_{pr}(\beta) := \begin{cases} l_c(W) & \text{if } f^+(\beta) < l_c(W) \\ u_c(W) & \text{if } f^+(\beta) > u_c(W) \\ f^+(\beta) & \text{else} \end{cases} \quad (15)$$

**Initialization** The BiSE layer performs convolutions with a smooth threshold function as the activation, resulting in values in the range of  $[0, 1]$ . Since we have reparametrized the weights to be positive, the classical initialization proposed in [7], which is tailored for ReLU activation and includes negative weights, needs to be adapted. We ensure that the gradients do not vanish during initialization, especially when stacking BiSE neurons in a deep network. Inspired by [7], we sample uniform weights with an adjusted distribution that maintains a constant variance. Additional details can be found in Appendix A.

### 3. Binarization

Binarization of a neural network involves converting the real-valued weights and activations, typically stored as 32-bit floats, into binary variables represented as 1-bit booleans. While the conventional approach results in variables in  $\{-1, 1\}$  [26], which is not suitable for learning morphological operations, we instead utilize  $\{0, 1\}$ .

BiMoNNs inherently correspond to binarized networks, making the BiSE neuron a natural framework for binarization when dealing with binary inputs. If a specialized hardware tailored for morphological operations is available, it can offer significant improvements in efficiency and performance, facilitating the binarization process. Alternatively, dilation and erosion can be expressed using binary-weighted thresholded convolutions.

In our approach, binarization occurs after the training phase. We present two types of binarization for the BiSE neuron: the exact method (as introduced in [2]), when the BiSE neuron is activated, and two novel approximated methods. Then, we sequentially binarize the entire network.

#### 3.1. Exact BiSE Binarization

The real-value operations performed by an activated Binary Structuring Element (BiSE) in the almost binary space can be replaced with binary morphological operations on the binary space after thresholding by 0.5, without sacrificing performance (as per Theorem 2.3). To determine if a BiSE is activated and which operation it corresponds to, we introduce Proposition 3.1, which provides a linear complexity method for extraction.

**Proposition 3.1** (Linear Check). *Let us assume the BiSE of weights  $W(\omega)$  and  $B(\beta)$  is activated for  $\psi$  with SE  $S \subset \Omega$  for almost binary images  $\mathcal{I}(\delta)$ . Then  $S = (W(\omega) > \tau_\psi)$  with*

$$\tau_\oplus := \frac{1}{\frac{1}{2} + \delta} \left( B(\beta) - \sum_{w \in W(\omega)} [w]_- \right) \quad (16)$$

$$\tau_\ominus := \frac{1}{\frac{1}{2} + \delta} \left( \sum_{w \in W(\omega)} [w]_+ - B(\beta) \right) \quad (17)$$

Given a BiSE neuron  $\chi$  and an almost binary output in  $\mathcal{I}(\delta)$ , we check if  $\chi$  is activated for  $S_{\oplus}$  or  $S_{\ominus}$ , where  $S_{\oplus} = (W(\omega) > \tau_{\oplus})$  and  $S_{\ominus} = (W(\omega) > \tau_{\ominus})$ . If yes, we binarize by replacing  $\chi$  with the corresponding morphological operator. If no, we use proposition 3.1 to confirm that  $\chi$  is not activated, and we approximate the binarization using the methods in section 3.2. The exact method requires only the computation of  $L_{\oplus}, U_{\oplus}, L_{\ominus}, U_{\ominus}$  and at most  $\mathcal{O}(|\Omega_S|)$  operations.

### 3.2. Approximate BiSE Binarization

In practice, BiSE are rarely activated, necessitating an approximate binarization method. Let  $(\widehat{\mathbf{W}}, \widehat{b}, \widehat{p}) := (\mathbf{W}(\widehat{\omega}), B(\widehat{\beta}), \widehat{p})$  be the learned reparametrized parameters.

#### 3.2.1 Projection onto activable parameters

To find the closest morphological operation, we minimize the Euclidean distance  $d$  for a given  $\psi \in \{\oplus, \ominus\}$  and the set  $A_{\psi, S}$  of activable parameters:

$$A_{\psi, S} := \left\{ (\mathbf{w}, b) \in \mathbb{R}^{\Omega} \times \mathbb{R} \mid L_{\psi}(\mathbf{w}, S) < b < U_{\psi}(\mathbf{w}, S) \right\} \quad (18)$$

$$\underset{S \subset \Omega, \psi \in \{\oplus, \ominus\}}{\text{minimize}} \quad d\left((\widehat{\mathbf{W}}, \widehat{b}), A_{\psi, S}\right) \quad (19)$$

For each set  $A_{\psi}(S)$  corresponding to a possible morphological operation, we find the smallest distance for each  $(S, \psi)$  and apply complementation if  $\widehat{p} < 0$ . The following proposition allows linear search instead of exponential.

**Proposition 3.2.** *If  $S^*, \psi^*$  minimize  $d((\widehat{\mathbf{W}}, \widehat{b}), A_{\psi, S})$ , then  $S^* = (\widehat{\mathbf{W}} \geq \min_{S^*} \widehat{\mathbf{W}}_s)$*

Proposition 3.1 guarantees that the SE is a set of thresholded weights when the weights are activated. Proposition 3.2 ensures that this property is preserved for the optimal SE even when the weights are not activated. Thus, we only need to compute the distance to all possible sets of thresholded weights, denoted as  $S_k := (\widehat{\mathbf{W}} \geq \widehat{\mathbf{W}}_k)$ , and select the smallest distance. To compute the distance for  $\psi$  and  $S$  fixed, we solve the following optimization problem.

$$\begin{aligned} & \underset{(\mathbf{w}, b) \in \mathbb{R}_+^{\Omega} \times \mathbb{R}}{\text{minimize}} \quad \frac{1}{2} \sum_{i \in \Omega} (W_i - \widehat{\mathbf{W}}_i)^2 + \frac{1}{2} (b - \widehat{b})^2 \\ & \text{subject to} \quad \begin{cases} L_{\psi}(\mathbf{w}, S) - b \leq 0 \\ b - U_{\psi}(\mathbf{w}, S) \leq 0 \end{cases} \quad (20) \end{aligned}$$

When the initial weights  $\widehat{\mathbf{W}}$  are positive, the projected weights are also positive. Consequently, the constraints can

be rewritten for dilation and erosion as follows:

$$\oplus \begin{cases} \sum_{k \in \Omega \setminus S} W_k - b \leq 0 \end{cases} \quad (21)$$

$$\begin{cases} \forall s \in S, b \leq W_s \end{cases} \quad (22)$$

$$\begin{cases} \forall k \in \Omega \setminus S, -W_k \leq 0 \end{cases} \quad (23)$$

$$\ominus \begin{cases} b - \sum_{s \in S} W_s \leq 0 \end{cases} \quad (24)$$

$$\begin{cases} \forall s \in S, \sum_{i \in \Omega} W_i - \mathbf{W}_s \leq b \end{cases} \quad (25)$$

$$\begin{cases} \forall k \in \Omega \setminus S, -W_k \leq 0 \end{cases} \quad (26)$$

These new constraints are then linear. By utilizing the positive reparametrization technique (as described in §2.4), we can compute the distance to any activable parameter set  $A_{\psi, S}$  by solving a QP problem, using the OSQP solver [25]. This needs to be done for all possible sets of thresholds  $S_k$ , of which there are  $|\Omega|$ . For a single layer with 4096 input and output neurons, the computation would take up to 28 days (on a Intel(R) Xeon(R) W-2265 CPU, 3.50GHz). Future work may involve finding an analytically computable form for efficient distributed computing. Alternatively, we introduce the following approximation technique.

#### 3.2.2 Projection onto constant weights

We use a similar technique to [17]. First, we define  $\widetilde{A}_S$  the set of constant weights over  $S$ , and replace  $d((\widehat{\mathbf{W}}, \widehat{b}), A_{\psi, S})$  with  $d(\widehat{\mathbf{W}}, \widetilde{A}_S)$ .

$$\widetilde{A}_S := \{\theta \cdot \mathbb{1}_S \mid \theta > 0\} \quad (27)$$

$$d(\widehat{\mathbf{W}}, \widetilde{A}_S) = \sum_{i \in \Omega} \widehat{\mathbf{W}}_i^2 - \frac{1}{|S|} \left( \sum_{s \in S} \widehat{\mathbf{W}}_s \right)^2 \quad (28)$$

Similarly to proposition 3.2, we can prove that the optimal  $S^*$  is a set of thresholded weights. The analytical form in 28 allows for efficient computation of  $S^*$  in distributed systems, significantly faster than the first method. For a layer with 500 input and output channels, this step takes less than 3 seconds. Once  $S^*$  is obtained, the bias term helps determine  $\psi \in \{\oplus, \ominus\}$ , based on Theorem 2.3. If  $\widehat{b} > \sum_{\widehat{\mathbf{W}}} w/2$ , the operation is an erosion; otherwise, it is a dilation.

### 3.3. BiMoNN binarization

The core of the successive binarization is Theorem 2.3. To simplify, we suppose that a BiMoNN is a succession of BiSE. If the first BiSE is activated, then with a binary input (e.g. almost binary with  $\delta_0 = \frac{1}{2}$ ), the output is almost binary of known parameter  $\delta_1$ . If the next BiSE is activated for the parameter  $\delta_1$ , its output is also activated for parameter  $\delta_2$ , and so on. Hence, every BiSE operation on the almost binary space is equivalent to the morphological operation on the binary space. In case one BiSE is not activated,

its output is not on the almost binary space, breaking the exact equivalence between BiSE and morphology. We apply an approximate method (projection §3.2.1 if small network, otherwise fast projection §3.2.2), and suppose that the input for the next BiSE is binary.

## 4. Morphological Regularization

The binarization schema, as described in §3, is separate from the training process. During standard loss optimization with classical gradient descent, there is no explicit constraint that makes the network behave morphologically. Consequently, the network may not tend to a morphological operation: BiSE operators may not be activated and the weights may stay far from their respective projection space, resulting in potential errors in the approximate binarization process compared to the floating-point operator. To encourage the network to exhibit a more morphological behavior, we propose the inclusion of a regularization term in the loss, denoted as  $\mathcal{L}_{morpho}$ . The loss function now becomes:

$$\mathcal{L} = \mathcal{L}_{data} + c \cdot \mathcal{L}_{morpho} \quad (29)$$

$\mathcal{L}_{data}$  represents the loss used for the data-driven task (e.g. Cross-Entropy Loss for classification), and  $c$  is the hyperparameter controlling the strength of the regularization term. To define the regularization term, we reuse the two approximate binarization techniques defined in section 3.2.

### 4.1. Regularization onto activable parameters

A first idea is to reduce the distance to the closest set  $A_{\psi,S}$  defined in (18) for each BiSE neuron. Let  $(\mathbf{W}, b) := (W(\omega), B(\beta))$  be the weights in a given iteration. Then:

$$\mathcal{L}_{morpho} = \mathcal{L}_{acti} := \min_{S,\psi} d\left((\mathbf{W}, b), A_{\psi,S}\right) \quad (30)$$

To do this, we must compute this distance in a differentiable fashion. We proceed in two steps: first, we compute the optimal  $(S^*, \psi^*)$  as in §3.1, by checking all possible thresholded set of weights and solving the corresponding QP with OSQP, with the Lagrangian dual method. This yields the best  $(\mathbf{W}^*, b^*)$  as well as the Lagrangian dual values, from which we deduce the differentiable form of the distance. If  $\psi^* = \oplus$ , let  $\lambda^*$  be the dual value for the constraint (21) and

$$\mathbb{T} := \{t \in S^* \mid \mathbf{W}_t \leq b^*\} \quad (31)$$

$$\mathbb{K} := \{k \in \Omega \setminus S^* \mid \mathbf{W}_k \leq \lambda^*\} \quad (32)$$

$$\mathbb{K} := (\Omega \setminus S^*) \setminus \mathbb{K} \quad (33)$$

$$D := |\mathbb{K}|(|\mathbb{T}| + 1) + 1, \quad (34)$$

then we can show that we obtain the following differentiable

expressions for  $(\mathbf{W}^*, b^*)$ .

$$b^* = \frac{1}{D} \left( \sum_{j \in \mathbb{K}} \mathbf{W}_j + |\mathbb{K}| \left( \sum_{t \in \mathbb{T}} \mathbf{W}_t + b \right) \right) \quad (35)$$

$$\forall j \in \mathbb{K}, \mathbf{w}_j^* = W_j + \frac{1}{D} \left( \sum_{t \in \mathbb{T}} W_t + b - (|\mathbb{T}| + 1) \sum_{i \in \mathbb{K}} W_i \right) \quad (36)$$

$$\forall k \in \mathbb{K}, \mathbf{W}_k^* = 0 \quad (37)$$

$$\forall t \in \mathbb{T}, \mathbf{W}_t^* = b^* \quad (38)$$

$$\forall s \in S^* \setminus \mathbb{T}, \mathbf{W}_s^* = \mathbf{W}_s. \quad (39)$$

Then, we have a differentiable expression for the loss.

$$\mathcal{L}_{acti} = \sum_{i \in \Omega} (W_i - \mathbf{w}_i^*)^2 - (b - b^*)^2 \quad (40)$$

However, the computational burden described in §3.1 persists: the first step of computing  $S^*$  is too long in practice.

### 4.2. Regularization onto constant set

Instead of trying to enforce a fully morphological network, we can encourage the weights to stay in the set of constant weights  $\hat{A}_S$  defined in (27). We proceed in two steps: we find the best  $S^*$  in the same way as in §3.2.2, i.e. by computing the distance  $d(\hat{A}_S, \mathbf{W})$  defined in (28) for all set of thresholded weights, and selecting the smallest distance. Then, a differentiable expression for the distance is:

$$\mathcal{L}_{morpho} = \mathcal{L}_{exact} := \sum_{i \in \Omega} \mathbf{W}_i - \frac{1}{|S^*|} \left( \sum_{s \in S^*} \mathbf{W}_s \right)^2 \quad (41)$$

Computing the distance for all set of thresholded weights still takes significant time, and in our experimentation, this slows the training by up to 80×. Instead, we propose to use the technique introduced in [17]. If we assume that the weights follow a uniform or normal distribution, we can approximate the optimal  $S^* \simeq (\mathbf{W} > \tau)$  with the following thresholds:

$$\text{Uniform } \tau_u := \frac{2}{3} \left( \frac{1}{|\Omega|} \sum_{i \in \Omega} \mathbf{W}_i \right) \quad S_u := (\mathbf{W} > \tau_u) \quad (42)$$

$$\text{Normal } \tau_n := \frac{3}{4} \left( \frac{1}{|\Omega|} \sum_{i \in \Omega} \mathbf{W}_i \right) \quad S_n := (\mathbf{W} > \tau_n) \quad (43)$$

From this, we can define two regularization loss which can be computed without slowing the training down.

$$\mathcal{L}_{morpho} = \mathcal{L}_{unif} := \sum_{i \in \Omega} \mathbf{W}_i - \frac{1}{S_u} \left( \sum_{s \in S_u} \mathbf{W}_s \right)^2 \quad (44)$$

$$\mathcal{L}_{morpho} = \mathcal{L}_{normal} := \sum_{i \in \Omega} \mathbf{W}_i - \frac{1}{S_n} \left( \sum_{s \in S_n} \mathbf{W}_s \right)^2 \quad (45)$$

## 5. Experiments

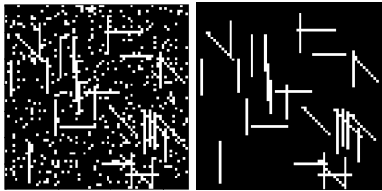
In this section, we empirically validate the capabilities of BiMoNNs in learning a binarized morphological pipeline through a denoising task, without the need for regularization. We also evaluate the model and regularization techniques on the MNIST classification task.

### 5.1. Binary Denoising

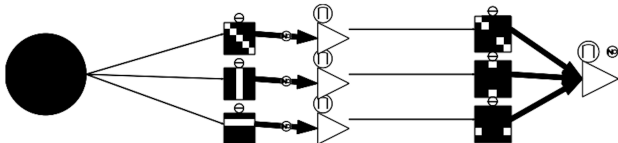
We generate a second dataset to evaluate the denoising capacity of BiMoNNs. The target images in this dataset consist of randomly-oriented segments with width  $h$ , with added Bernoulli noise. To filter these images, an MM expert would use a union of opening operations, where the SEs are segments with width 1 and angle one of  $(0^\circ, 90^\circ, -45^\circ)$ . The SEs should be longer than the noise and shorter than the smallest stick in the target image (usually a length of 5). Examples are given in figure 3a.

Our architecture uses two consecutive BiSEL layer of kernel size 5 and 3 hidden channels (see figure 3b). We optimize the MSE Loss, with an initial learning rate of 0.01. We train over 6000 iterations and halve the learning rate after 700 iterations with non-diminishing loss. We stop once the loss does not decrease after 2100 iterations. We employ a positive reparametrization for the bias and a dual reparametrization for the weights, and binarize with the projection onto activable parameters.

The network achieves excellent denoising performance, with a DICE score of 97.5%. The remaining 2.5% discrepancy is due to artifacts between the sticks that cannot be denoised using an opening operation. The binarized network (Figure 3b) accurately learns the intersection of three openings (which remains an opening) the same way a human expert would combine such operators to achieve the denoising task optimally. Additionally, 4 out of the 6 BiSE are activated during the process. This experiment shows that our network can learn accurate and interpretable composition of morphological operators.



(a) Input-output example.



(b) Binarization of the network

### 5.2. Classification

We conduct classification experiments on the MNIST dataset [16]. All images are thresholded at 128. Our BiMoNN model comprises one hidden DenseLUI layer with 4096 neurons. To handle the large number of parameters, we adopt the fast projection defined in §3.2. We compare the classification accuracy of our float and binarized models against the SOTA and baseline models with fully connected layers and 1D batch normalization [11], employing  $\frac{1}{2}(\tanh(\cdot) + 1)$  as the activation layer. The accuracy results are summarized in Table 1.

In our framework, binarizing the weights also entails binarizing the activations. Consequently, binarizing the last layer would yield binary decision outputs for each output neuron, possibly leading to multiple labels with a score of 1. To overcome this issue, we refrain from binarizing the last layer, thus retaining the real-valued activations. This decision affects a negligible proportion of parameters ( $\simeq 0.1\%$ ).

In traditional classification neural networks, the softmax activation is commonly used at the end of the last layer to produce the final probability distribution over the classes. However, in the BiMoNN architecture, we utilize the same activation function as the hidden layers, which is the normalized tanh. Additionally, we compare the performance of our BiMoNN model when replacing the last normalized tanh activation with a softmax layer. When using the normalized tanh,  $\mathcal{L}_{data}$  is the Binary Cross-Entropy loss. When using the softmax, we use the Cross-Entropy loss.

$$\mathcal{L}_{BCE}(\hat{\mathbf{y}}_i, \mathbf{y}_i^*) := \sum_{c=1}^{10} \mathbf{y}_i^* \log(\hat{\mathbf{y}}_i) + (1 - \mathbf{y}_i^*) \log(1 - \hat{\mathbf{y}}_i) \quad (46)$$

$$\mathcal{L}_{CE}(\hat{\mathbf{y}}_i, \mathbf{y}_i^*) := \sum_{c=1}^{10} \mathbf{y}_i^* \log(\hat{\mathbf{y}}_i) \quad (47)$$

We conduct a comprehensive random search to identify the optimal hyperparameter configuration for the Binary Morphological Neural Network (BiMoNN). The hyperparameters explored include the learning rate, last activation function (Softmax layer vs. normalized tanh), positive vs no reparametrization for weights, and several bias reparametrization schemas (no reparametrization, positive, positive reparam, and positive projected). Additionally, we investigate regularization losses, such as no regularization,  $\mathcal{L}_{exact}$ ,  $\mathcal{L}_{uni}$ , and  $\mathcal{L}_{nor}$ . If regularization is applied, only positive weight reparametrization is considered. We vary the coefficient  $c$  in the regularization loss and explore different batch value starting time for when we start applying regularization during training. For each regularization schema, we select the model with the best binary validation accuracy, and the corresponding results are displayed in Table 1. Detailed hyperparameter configurations and hy-

perparameters study are provided in appendix B.

Table 1: Accuracy error on test set for MNIST classification, with float error  $\mathbb{R}$  and binarized error  $\mathbb{B}$ .

	Architecture	Params	$\mathbb{R}$	$\mathbb{B}$
Ours	DLUI ( $W = \text{Id}$ )	3.3 M	<b>2.2%</b>	90.2%
	DLUI (No Regu)	3.3 M	4.6%	10.1%
	DLUI $\mathcal{L}_{\text{exact}}$	3.3 M	4.0%	7.3%
	DLUI $\mathcal{L}_{\text{unif}}$	3.3 M	3.6%	<b>4.5%</b>
	DLUI $\mathcal{L}_{\text{normal}}$	3.3 M	2.8%	4.6%
SOTA	EP 1fc [15]	3.3 M	-	2.8%
	BinConnect [5]	10 M	-	<b>1.3%</b>
	BNN [10]	10 M	-	1.4%
Float	FC (4096)	3.3 M	1.5 %	-
	FC (2048x3) [10]	10 M	<b>1.3%</b>	-

Applying the softplus reparametrization to the weights led to a slight increase in the floating-point error (2.2% vs. 2.8%). Similar findings were observed in [20] for non-negative neural networks in a different task. Generally, positive neural networks exhibit lower accuracy but offer enhanced robustness and interpretability [4]. In our case, it significantly improved the binarized results, along with a substantial increase in the rate of activated BiSE neurons, rising from a median of 1.5% to 10% with softplus. Without imposing positivity, the binarized network performed randomly.

We analyze the impact of regularization on the performance of the binarized model, which improves as expected. The float accuracy also increases, given that we select the model with the best binary accuracy on validation. Surprisingly,  $\mathcal{L}_{\text{unif}}$  and  $\mathcal{L}_{\text{normal}}$  outperform  $\mathcal{L}_{\text{exact}}$ , despite being designed as approximations. This discrepancy might be due to the number of searches performed:  $\mathcal{L}_{\text{exact}}$  performed only 42 searches, while other configurations went through 100 searches. However, we have not yet achieved parity with the baseline for the float model or reached the state-of-the-art for the binarized model. With 4.5% error compared to 2.8% for the same number of parameters, this emphasizes the need for improved architecture, better regularization techniques, or exploration of alternative optimization methods.

### 5.3. Discussion

The state-of-the-art BWNN methods commonly rely on the XNOR operator to emulate multiplications. However, this algebraic framework proves unsuitable for morphological operators, as it contradicts the set-theoretical principles of morphological operations. In our experiments, we observed that the BNN operator [10] failed to learn even the simplest dilation operator. Furthermore, the performance of the state-of-the-art method on the denoising task was un-

satisfactory, with a DICE coefficient of only approximately 0.3, indicating the need for improved approaches in handling morphological operations.

In contrast, our findings reveal that the float BiMoNN exhibits enhanced binarization capabilities when trained to closely approximate a set of morphological operators. As a result, the float BiMoNN naturally acquires morphological properties, leading to a more effective subsequent binarization process. However, when applied to the classification of the MNIST dataset, the resulting float BiMoNN does not retain morphological characteristics, causing a noticeable performance degradation after binarization. To address this issue, we emphasize the importance of positive reparametrization and applying morphological regularization. By incorporating these techniques, we significantly improved the model’s overall performance and mitigate the accuracy loss upon binarization. This shows the potential of our proposed BiMoNN framework in leveraging morphological properties and offers insights into the development of more effective BiMoNN models for many and diverse tasks.

## 6. Conclusion

In this paper, we have presented a novel, mathematically justified approach to binarize neural networks using the Binary Morphological Neural Network (BiMoNN), achieved by leveraging mathematical morphology. Our proposed method establishes a direct link between deep learning and mathematical morphology, enabling binarization of a wider set of architectures, without performance loss under specific activation conditions and providing an approximate solution when these conditions are not met.

Through our experiments, we have demonstrated the effectiveness of our approach in learning morphological operations and achieving high accuracy in denoising tasks, surpassing state-of-the-art techniques that rely on the straight-through estimator (STE). Furthermore, we proposed and evaluated three practical regularization techniques that aid in converging to a morphological network, showcasing their efficacy in a classification task. Additionally, we introduced a fourth regularization technique that, though promising in theory, currently faces computational challenges. We will address these shortcomings in future work.

Despite promising results, there is still room for enhancing both the floating point and binary modes of our network. In future work, diverse architectures, such as incorporating convolution layers, could be explored to further improve the performance and applicability of BiMoNN. Overall, our research lays the foundation for advancing the field of binarized neural networks with a morphological perspective, offering valuable insights into developing more powerful and efficient models for a wide range of tasks.



## References

- [1] Jesus Angulo. Some open questions on morphological operators and representations in the deep learning era. In *International Conference on Discrete Geometry and Mathematical Morphology*, pages 3–19. Springer, 2021. 1
- [2] Theodore Aouad and Hugues Talbot. Binary morphological neural network. In *2022 IEEE International Conference on Image Processing (ICIP)*, pages 3276–3280, 2022. 1, 2, 4
- [3] Yoshua Bengio, Nicholas Léonard, and Aaron C. Courville. Estimating or propagating gradients through stochastic neurons for conditional computation. *CoRR*, abs/1308.3432, 2013. 1
- [4] Jan Chorowski and Jacek M Zurada. Learning understandable neural networks with nonnegative weight constraints. *IEEE transactions on neural networks and learning systems*, 26(1):62–69, 2014. 8
- [5] Matthieu Courbariaux, Yoshua Bengio, and Jean-Pierre David. Binaryconnect: Training deep neural networks with binary weights during propagations. In C. Cortes, N. Lawrence, D. Lee, M. Sugiyama, and R. Garnett, editors, *Advances in Neural Information Processing Systems*, volume 28. Curran Associates, Inc., 2015. 1, 8
- [6] Gianni Franchi, Amin Fehri, and Angela Yao. Deep morphological networks. *Pattern Recognition*, 102:107246, 2020. 1
- [7] Kaiming He, Xiangyu Zhang, Shaoqing Ren, and Jian Sun. Delving deep into rectifiers: Surpassing human-level performance on imagenet classification. In *2015 IEEE International Conference on Computer Vision (ICCV)*, pages 1026–1034, 2015. 4
- [8] Xiangyu He, Zitao Mo, Ke Cheng, Weixiang Xu, Qinghao Hu, Peisong Wang, Qingshan Liu, and Jian Cheng. Proxybnn: Learning binarized neural networks via proxy matrices. In *Computer Vision—ECCV 2020: 16th European Conference, Glasgow, UK, August 23–28, 2020, Proceedings, Part III 16*, pages 223–241. Springer, 2020. 1
- [9] Romain Hermay, Guillaume Tochon, Élodie Puybareau, Alexandre Kirszenberg, and Jesús Angulo. Learning grayscale mathematical morphology with smooth morphological layers. *Journal of Mathematical Imaging and Vision*, pages 1–18, 2022. 1
- [10] Itay Hubara, Matthieu Courbariaux, Daniel Soudry, Ran El-Yaniv, and Yoshua Bengio. Binarized neural networks. *Advances in neural information processing systems*, 29, 2016. 8
- [11] Sergey Ioffe and Christian Szegedy. Batch normalization: Accelerating deep network training by reducing internal covariate shift. In *International conference on machine learning*, pages 448–456. pmlr, 2015. 7
- [12] Minje Kim and Paris Smaragdis. Bitwise neural networks. *arXiv preprint arXiv:1601.06071*, 2016. 1
- [13] Diederik P. Kingma and Jimmy Ba. Adam: A method for stochastic optimization, 2017. 3
- [14] Branislav Kisanin and Dan Schonfeld. A fast thresholded linear convolution representation of morphological operations. *IEEE Transactions on Image Processing*, 3(4):455–457, 1994. 1
- [15] Jérémie Laydevant, Maxence Ernoult, Damien Querlioz, and Julie Grollier. Training dynamical binary neural networks with equilibrium propagation. *CoRR*, abs/2103.08953, 2021. 8
- [16] Yann LeCun. The mnist database of handwritten digits. <http://yann.lecun.com/exdb/mnist/>, 1998. 2, 7
- [17] Fengfu Li, Bin Liu, Xiaoxing Wang, Bo Zhang, and Junchi Yan. Ternary weight networks. *arXiv preprint arXiv:1605.04711*, 2016. 5, 6
- [18] Jonathan Masci, Jesús Angulo, and Jürgen Schmidhuber. A learning framework for morphological operators using counter-harmonic mean. In *International Symposium on Mathematical Morphology and Its Applications to Signal and Image Processing*, pages 329–340. Springer, 2013. 1
- [19] Ranjan Mondal, Moni Shankar Dey, and Bhabatosh Chanda. Image restoration by learning morphological opening-closing network. *Mathematical Morphology-Theory and Applications*, 4(1):87–107, 2020. 1
- [20] Ana Neacsu, Jean-Christophe Pesquet, and Corneliu Burileanu. Accuracy-robustness trade-off for positively weighted neural networks. In *ICASSP 2020-2020 IEEE International Conference on Acoustics, Speech and Signal Processing (ICASSP)*, pages 8389–8393. IEEE, 2020. 8
- [21] Mohammad Rastegari, Vicente Ordonez, Joseph Redmon, and Ali Farhadi. Xnor-net: Imagenet classification using binary convolutional neural networks. In Bastian Leibe, Jiri Matas, Nicu Sebe, and Max Welling, editors, *Computer Vision – ECCV 2016*, pages 525–542, Cham, 2016. Springer International Publishing. 1
- [22] David E. Rumelhart, Geoffrey E. Hinton, and Ronald J. Williams. Learning Representations by Back-propagating Errors. *Nature*, 323(6088):533–536, 1986. 4
- [23] J. Serra. *Image Analysis and Mathematical Morphology*. Academic Press, 1982. 1
- [24] Yucong Shen, Xin Zhong, and Frank Y Shih. Deep morphological neural networks. *arXiv preprint arXiv:1909.01532*, 2019. 1
- [25] B. Stellato, G. Banjac, P. Goulart, A. Bemporad, and S. Boyd. OSQP: an operator splitting solver for quadratic programs. *Mathematical Programming Computation*, 12(4):637–672, 2020. 5
- [26] Chunyu Yuan and Sos S Aghaian. A comprehensive review of binary neural network. *arXiv preprint arXiv:2110.06804*, 2021. 4
- [27] Shuchang Zhou, Zekun Ni, Xinyu Zhou, He Wen, Yuxin Wu, and Yuheng Zou. Dorefa-net: Training low bitwidth convolutional neural networks with low bitwidth gradients. *CoRR*, abs/1606.06160, 2016. 1

## A. Initialization

### A.1. Initialization

In this section, we investigate the initialization of the BiSE neuron. Let us suppose that we stack  $L \in \mathbb{N}^*$  BiSE neurons one after the other.

**Notations** Let  $l \in \llbracket 1, L \rrbracket$  be the layer number. Let  $\mathbf{W}_l \in \mathbb{R}^{\Omega_S}$  be the random set of weights of this layer. Let  $b_l \in \mathbb{R}$  be the bias (not random). Let  $\mu_l := \mathbb{E}(\mathbf{W}_l)$  and  $\sigma_l := \text{Var}(\mathbf{W}_l)$ . Let  $\mathbf{x}_0 \in \{0, 1\}^{\Omega_I}$  be the input image, and for  $l \in \llbracket 1, K \rrbracket$ , let  $\mathbf{x}_l$  be the output of the  $l^{\text{th}}$  layer:  $\mathbf{x}_l := \xi(\mathbf{y}_l) \in [0, 1]^{\Omega_I}$  with  $\mathbf{y}_l := \mathbf{x}_{l-1} \circledast \mathbf{W}_l - b_l \in \mathbb{R}^{\Omega_I}$  such that for  $j \in \Omega_I$ ,  $\mathbf{y}_l(j) = \sum_{i \in \Omega_S} \mathbf{W}_l(i) \mathbf{x}_{l-1}(j-i) - b_l$ . Let  $n_l = |\mathbf{W}_l|$ .

### Assumptions

1. For  $l \in \llbracket 1, L \rrbracket$ , the  $(\mathbf{W}_l(i))_{i \in \Omega_S^l}$  are independent, identically distributed (IID)
2. For  $l \in \llbracket 1, L \rrbracket$ , the  $(\mathbf{x}_l(i))_{i \in \Omega_I}$  are IID
3. For  $l \in \llbracket 1, L \rrbracket$ ,  $\mathbb{E}[\mathbf{y}_l] = 0$  and  $p(\mathbf{y}_l)$  is symmetrical around 0
4. For  $(l, i, j) \in (\llbracket 1, L \rrbracket \times \Omega_S \times \Omega_I)$ ,  $\mathbf{W}_l(i)$  and  $\mathbf{x}_{l-1}(j-i)$  are independent

Under these assumptions, we can drop the  $i$  and  $j$  index and rewrite  $\mathbf{y}_l = \sum \mathbf{W}_l \mathbf{x}_{l-1} - b_l$ , with implicit indexing. The same goes for  $\mathbf{x}_l$ .

According to Fubini-Lebesgue theorem, and using assumption 3, we have  $\mathbb{E}[\mathbf{x}_l] = \mathbb{E}[\xi(\mathbf{y}_l)] = \xi(\mathbb{E}[\mathbf{y}_l]) = 0.5$ .

**Bias computation** We have,  $\forall l \in \llbracket 1, K \rrbracket$ ,  $\mathbb{E}[\mathbf{y}_l] = n_l \mathbb{E}[\mathbf{W}_l] \mathbb{E}[\mathbf{x}_{l-1}] - b_l$ . We use the unbiased estimator to compute the mean, by summing all the weights of the layer:  $\mu_l := \frac{1}{n_l} \sum_{w \in \mathbf{W}_l} w$ . Therefore, with  $\mathbb{E}(\mathbf{x}_0)$  the mean of the inputs:

$$b_1 = \mathbb{E}(\mathbf{x}_0) \sum_{w \in \mathbf{W}_1} w \quad (48)$$

$$\forall l \in \llbracket 2, K \rrbracket, b_l = \frac{1}{2} \sum_{w \in \mathbf{W}_l} w \quad (49)$$

In some cases, we initialize the scaling factor  $p = 0$  to avoid bias towards applying complementation or not. Then, this initialization leads to a point with zero grad (see annexe A.2 for details). Therefore, we add some noise to the bias:

$$\forall l \geq 2, B_l = \frac{1}{2} \sum_{W_l} w + \mathcal{U}(-\epsilon_{bias}, \epsilon_{bias}) \quad (50)$$

$$B_1 = \mathbb{E}(\mathbf{x}_0) \sum_{W_1} w + \mathcal{U}(-\epsilon_{bias}, \epsilon_{bias}) \quad (51)$$

$\epsilon_{bias}$  depends on the length of the network. It is set between  $[10^{-4}, 10^{-2}]$ .

**Variance computation** We find a recurrence relation between  $\text{Var}(\mathbf{y}_l)$  and  $\text{Var}(\mathbf{y}_{l-1})$ . To simplify the computations, let  $p' = \frac{d\xi(p \cdot x)}{dx}(0)$  be the tangent at 0, and let us assume that  $p' > 0$ . We approximate the smooth threshold by a piece-wise linear function:

$$\xi(u) \simeq \left(\frac{1}{2} + p\right) \mathbb{1}_{]-\frac{1}{2p}, \frac{1}{2p}[}(u) + \mathbb{1}_{] \frac{1}{2p}, +\infty[}(u) \quad (52)$$

$$\mathbb{E}[\mathbf{x}_l^2] = \mathbb{E}[\xi(\mathbf{y}_l)^2] \quad (53)$$

$$\mathbb{E}[\mathbf{x}_l^2] \simeq p'^2 \int_{-\frac{1}{2p'}}^{\frac{1}{2p'}} y^2 p(\mathbf{y}_l) d\mathbf{y}_l + p' \int_{-\frac{1}{2p'}}^{\frac{1}{2p'}} \mathbf{y}_l p(\mathbf{y}_l) d\mathbf{y}_l + \frac{1}{2} \int_0^{+\infty} p(\mathbf{y}_l) d\mathbf{y}_l + \frac{1}{2} \int_{\frac{1}{2p'}}^{+\infty} p(\mathbf{y}_l) d\mathbf{y}_l \quad (54)$$

$$= p'^2 \text{Var}(\mathbf{y}_l) + H(p') + \frac{1}{4} \quad (55)$$

$$\text{with } H(p') := \int_{\frac{1}{2p'}}^{+\infty} \left( \frac{1}{2} - 2p'^2 \mathbf{y}_l^2 \right) p(\mathbf{y}_l) d\mathbf{y}_l \quad (56)$$

By independence, we have

$$\frac{1}{n_l} \text{Var}(\mathbf{y}_l) = \text{Var}(\mathbf{W}_l \mathbf{x}_{l-1}) \quad (57)$$

$$= \sigma_l \text{Var}(\mathbf{x}_{l-1}) + \mathbb{E}[\mathbf{x}_{l-1}]^2 \sigma_l + \mu_l^2 \text{Var}(\mathbf{x}_{l-1}) \quad (58)$$

$$= \sigma_l [\mathbb{E}[\mathbf{x}_{l-1}^2] - \mathbb{E}[\mathbf{x}_{l-1}]^2] + \mathbb{E}[\mathbf{x}_{l-1}]^2 \sigma_l + \mu_l^2 [\mathbb{E}[\mathbf{x}_{l-1}^2] - \mathbb{E}[\mathbf{x}_{l-1}]^2] \quad (59)$$

$$= \mathbb{E}[\mathbf{x}_{l-1}^2] (\sigma_l + \mu_l^2) - \mu_l^2 \mathbb{E}[\mathbf{x}_{l-1}]^2 \quad (60)$$

$$\simeq p'^2 \text{Var}(\mathbf{y}_{l-1}) (\sigma_l + \mu_l^2) - \frac{1}{4} \mu_l^2 + (\sigma_l + \mu_l^2) \left( \frac{1}{4} + H(p') \right) \quad (61)$$

$$= p'^2 \text{Var}(\mathbf{y}_{l-1}) (\sigma_l + \mu_l^2) + G(p') \quad (62)$$

$$\text{with } G(p') := \frac{1}{4} \sigma_l + H(p') (\sigma_l + \mu_l^2) \quad (63)$$

If  $G(p') \geq 0$ , which is equivalent to  $H(p') \geq -\frac{\sigma_l}{4(\sigma_l + \mu_l^2)}$

$$\frac{1}{n_l} \text{Var}(\mathbf{y}_l) \leq p'^2 \text{Var}(\mathbf{y}_{l-1}) (\sigma_l + \mu_l^2) \quad (64)$$

We unroll the recursive relation. Let

$$V(p') := \text{Var}(\mathbf{y}_1) \prod_{k=1}^l p^2 n_k (\sigma_k + \mu_k^2) \quad (65)$$

Then

$$V(p') \leq \text{Var}(\mathbf{y}_l) \leq V(p') + \sum_{k=1}^L \frac{1}{4} \sigma_k \prod_{m=k}^l p^2 n_m (\sigma_m + \mu_m^2) \quad (66)$$

The right hand side of the inequality comes from the fact that  $H(p') \leq 0$ .

If  $G(p') \leq 0$ , which is equivalent to  $H(p') \leq -\frac{\sigma_l}{4(\sigma_l + \mu_l^2)}$ , we have:

$$0 \leq \text{Var}(\mathbf{y}_l) \leq V(p') \quad (67)$$

If the variance is equal to 0, then the output is constant: therefore, the gradient is 0 and we cannot learn the parameters. On the other hand, if the variance is too high, the model is poorly conditioned: we can expect the learning to be unstable.

If the number of layers is too big, the product term  $V(p')$  can either vanish or explode. To avoid variance exploding when  $G(p') \geq 0$ , and to avoid variance vanishing when  $G(p') \leq 0$ , we choose to ensure that the product is equal to 1 by imposing each term to be 1.

$$\forall l \in \llbracket 1, L \rrbracket, p'^2 n_l (\sigma_l + \mu_l^2) = 1 \quad (68)$$

$$\sigma_l = \frac{1}{p'^2 n_l} - \mu_l^2 \quad (69)$$

$$\forall l \in \llbracket 1, L \rrbracket, p'^2 n_l (\sigma_l + \mu_l^2) = 1 \quad (70)$$

The variance needs to be positive, which gives

$$\mu_l < \frac{1}{p'} \sqrt{\frac{1}{n_l}} \quad (71)$$

We have a range of possible means and variances. Let us choose a uniform distribution for  $\mathbf{W}_l$ . Then  $\mathbf{W}_k \sim \mathcal{U}(\mu_l - \sqrt{3\sigma_l}, \mu_l + \sqrt{3\sigma_l})$ . We want positive weights (see theorem 2.3), therefore we want  $\mu_l > \sqrt{3\sigma_l}$ , which gives

$$\mu_l > \frac{\sqrt{3}}{2p'} \sqrt{\frac{1}{n_l}} \quad (72)$$

Using equations 71 and 72, we choose  $\mu_l$  as the mean of the bounds:

$$\mu_l := \frac{\sqrt{3} + 2}{4p' \sqrt{n_l}} \quad (73)$$

**Role of the scaling factor  $p$**  Finally,  $p'$  is related to the value of  $p$ :  $p' = \frac{d(\xi(p;x))}{dx}(0) = p\xi'(0)$ . Ideally, to avoid bias towards applying complementation or not,  $p$  should be set at 0, therefore  $p' = 0$ . We consider that after the first few iterations,  $p \neq 0$ , and our computations become valid.

How to set  $p'$  in practice? We want the BiSE output to be in the full range  $[0, 1]$ . Let us suppose that after a few iterations,  $p = 1$ . With  $B_l = \sum_{w \in \mathbf{W}_l} w$ , the lowest output value is given by an image full of 0, giving  $\xi(-B_l)$ . The highest output is given by an image full of 1 and gives  $\xi(B_l)$ . Let  $h \in ]0, 1[$  (e.g.  $h = 0.95$ ). We want  $\xi(B) > h$ , which is the same as  $\xi(-B_l) < 1 - h$  thanks to the binary-odd property. By using the fact that  $\mu_l n_l \sim \sum_{w \in \mathbf{W}_l} w$ , we have:

$$\xi(B_l) \geq h \Leftrightarrow p' \leq \frac{\sqrt{3} + 2}{8\xi^{-1}(h)} \sqrt{n_l} \quad (74)$$

**Summary** With  $h = 0.95$ ,  $\epsilon_{bias} \in [10^{-4}, 10^{-2}]$  and  $p'_l := \frac{\sqrt{3} + 2}{8\xi^{-1}(h)} \sqrt{n_l}$ ,

$$\forall l \in \llbracket 1, L \rrbracket, \mu_l := \frac{\sqrt{3} + 2}{4p'_l \sqrt{n_l}} \quad (75)$$

$$\forall l \in \llbracket 1, L \rrbracket, \sigma_l := \frac{1}{p_l'^2 n_l} - \mu_l^2 \quad (76)$$

$$\forall l \in \llbracket 1, L \rrbracket, \mathbf{W}_l \sim \mathcal{U}(\mu_l - \sqrt{3\sigma_l}, \mu_l + \sqrt{3\sigma_l}) \quad (77)$$

$$\forall l \in \llbracket 1, L \rrbracket, p_l := 0 \quad (78)$$

$$\forall l \in \llbracket 2, L \rrbracket, b_l := \frac{1}{2} \sum_{w \in \mathbf{W}_l} w + \mathcal{U}(-\epsilon_{bias}, \epsilon_{bias}) \quad (79)$$

$$b_1 := \mathbb{E}(\mathbf{x}_0) \sum_{w \in \mathbf{W}_1} w + \mathcal{U}(-\epsilon_{bias}, \epsilon_{bias}) \quad (80)$$

We can approximate  $\mathbb{E}(\mathbf{x}_0)$  with the mean of a few samples, for example the first batch.

**Reparametrization** We computed the weights and biases of the convolution. In the BiSE definition 2.2, they correspond to  $W(\omega)$  and  $B(\beta)$ . The true initialization must be done on  $\omega$  and  $\beta$ . If  $W$  and  $B$  are invertible, the problem is solved:

$$\omega_l = W^{-1}(\mathbf{W}_l) \quad (81)$$

$$\beta_l = B^{-1}(b_l) \quad (82)$$

If the functions are not invertible, the study must be done case by case in order to find generative distributions for  $\omega_l$  and  $\beta_l$  that respects the resulting distributions for  $W(\omega_l)$  and  $B(\beta_l)$ .

**Dual reparametrization** For the dual reparametrization, we need to adapt the parameter  $K$ .

**Proposition A.1.** Let  $\sigma, \mu \in \mathbb{R}_+^2$  such that  $\mu - \sqrt{3\sigma} > 0$ . Let  $a \in \mathbb{R}_+^*$ . Let  $X_i \sim \mathcal{U}\left(a, a \frac{\mu + \sqrt{3\sigma}}{\mu - \sqrt{3\sigma}}\right)$  be a sequence of independent, identically distributed random variables,  $S_N = \sum_{i=1}^N X_i$ ,  $K_N = \mu \cdot N$  and  $W_{i,N} = K_N \frac{X_i}{S_N}$ . Then, almost certainly (a.c.)

$$W_{i,N} \xrightarrow[N \rightarrow \infty]{a.c.} \mathcal{U}(\mu - \sqrt{3\sigma}, \mu + \sqrt{3\sigma}) \quad (83)$$

*Proof.*

$$\mathbb{E}[|X_i|] = \mathbb{E}[X_i] = \frac{a}{2} \left(1 + \frac{\mu + \sqrt{3\sigma}}{\mu - \sqrt{3\sigma}}\right) = a \frac{\mu}{\mu - \sqrt{3\sigma}} < +\infty \quad (84)$$

Then, according to the strong law of large numbers,  $\frac{S_N}{N} \xrightarrow[N \rightarrow \infty]{a.c.} \mathbb{E}[X_i]$ . Then:

$$W_{i,N} = X_i \mu \frac{N}{S_N} \xrightarrow[N \rightarrow \infty]{a.c.} X_i \mu \frac{\mu - \sqrt{3\sigma}}{a\mu} = \frac{1}{a} (\mu - \sqrt{3\sigma}) X_i \sim \mathcal{U}(\mu - \sqrt{3\sigma}, \mu + \sqrt{3\sigma}) \quad (85)$$

□

Finally if we take  $a = \mu_k - \sqrt{3\sigma_k}$  the initialization becomes:

$$K = \mu_k \cdot n_k = 2 \cdot \xi^{-1}(h) \quad (86)$$

$$\mathbf{W}_k \sim \mathcal{U}(\mu_k - \sqrt{3\sigma_k}, \mu_k + \sqrt{3\sigma_k}) \quad (87)$$

$$K \frac{\mathbf{W}_k}{\sum_{w \in W_k} w} \sim_{n_k \rightarrow +\infty}^{a.c.} \mathcal{U}(\mu_k - \sqrt{3\sigma_k}, \mu_k + \sqrt{3\sigma_k}) \quad (88)$$

**Remark on bias initialization** Theorem 2.3 expresses the operation approximated by the BiSE depending on the bias. From the second to the last layer, the bias is initialized at the middle of both operation. Therefore, the BiSE are unbiased to learn either dilation or erosion.

However, for the first BiSE layer, the bias is initialized differently. If  $\mathbb{E}(\mathbf{x}_0) < \frac{1}{2}$ , then the bias indicates a dilation. We bias the BiSE to learn a dilation. This is explained by the assumption that the output must mean at  $\frac{1}{2}$ . If the input is a lower than  $\frac{1}{2}$ , we must increase its value. The same goes for the erosion: if the value of the input is too high, we reduce it by applying an erosion.

## A.2. Gradient Computation

Let  $\Gamma = \chi_L \circ \dots \circ \chi_1$  be a sequence of BiSE neurons, with parameters  $p_l$ ,  $b_l$  and  $\mathbf{W}_l$  for all layers  $l$ . We compute  $\mathcal{L}(\Gamma(X), Y)$  for one input sample. Let

$$\Pi_l := \partial_1 \mathcal{L}(\Gamma(X), Y) \left( \prod_{k=l+1}^N \text{diag}(\xi'(\chi_k)) p_k W_k \right) \quad (89)$$

We re-denote  $\mathbf{W}_l$  as the linear matrix such that  $\chi_{l-1} \circledast \mathbf{W}_l = \chi_{l-1} \mathbf{W}_l$ .

$$\frac{d\mathcal{L}}{dp_l} := \Pi_l \text{diag}(\xi'(\chi_l)) (\chi_{l-1} \mathbf{W}_l - b_l) \quad (90)$$

$$\frac{d\mathcal{L}}{db_l} := \Pi_l \text{diag}(\xi'(\chi_l)) (-p_l) \quad (91)$$

$$\frac{d\mathcal{L}}{d\mathbf{W}_l} := \Pi_l \text{diag}(\xi'(\chi_l)) p_l \phi_{l-1} \quad (92)$$

If for all  $l$ ,  $p_l = 0$ , then  $\frac{d\mathcal{L}}{db_l} = \frac{d\mathcal{L}}{d\mathbf{W}_l} = 0$ . Moreover, by initialization of the bias  $b_l$ , we have  $\chi_{l-1} \mathbf{W}_l - b_l = 0$ , leading to  $\frac{d\mathcal{L}}{dp_l} = 0$ . With our current initialization, all the gradients are equal to 0. Therefore, in practice, we add a uniform noise to the bias:

$$\forall l \geq 2, b_l = \frac{1}{2} \sum_{\mathbf{w}_l} w + \mathcal{U}(-10^{-4}, 10^{-4}) \quad (93)$$

$$B_1 = \mathbb{E}(X) \sum_{W_1} w + \mathcal{U}(-10^{-4}, 10^{-4}) \quad (94)$$

This will lead to  $p_l$  moving away from 0, which unblocks the other gradients as well. We introduce a small bias towards either dilation or erosion. However, its significance is negligible, and does not prevent from learning one operation or the other.

## B. Experiments

Table 2: Best set of hyperparameters for each architecture

Architecture	$W(\omega)$	$B(\omega)$	Coef Regu	Regu Delay	Learning Rate	Last Activation
DLUI ( $W = \text{Id}$ )	identity	identity	0	-	$6.2 \cdot 10^{-3}$	tanh
DLUI (No Regu)	positive	positive	0	-	$9.8 \cdot 10^{-2}$	tanh
DLUI $\mathcal{L}_{exact}$	positive	projected reparam	0.01	10000	$4.2 \cdot 10^{-2}$	softmax
DLUI $\mathcal{L}_{uni}$	positive	projected reparam	0.01	20000	$6.1 \cdot 10^{-2}$	softmax
DLUI $\mathcal{L}_{nor}$	positive	identity	0.001	10000	$5.4 \cdot 10^{-2}$	softmax

We perform a random search across a range of hyperparameters to identify the optimal configuration. The hyperparameters explored in the search are as follows:

- Learning rate between  $10^{-1}$  and  $10^{-3}$ .
- Last activation: Softmax layer vs Normalized tanh. If Softmax Layer, we use  $\mathcal{L}_{CE}$ , else we use  $\mathcal{L}_{BCE}$
- Applying the softplus reparametrization to the weights or not.
- The bias reparametrization schema between no reparametrization, positive, projected and projected reparam.
- Regularization loss: either no regularization, or the projection onto constant set (choose between  $\mathcal{L}_{exact}$ ,  $\mathcal{L}_{uni}$  and  $\mathcal{L}_{nor}$ ). If we apply regularization, then we also apply softplus reparametrization.
- If regularization: the coefficient  $c$  in the loss, either 0.01 or 0.001.
- If regularization: the number of batches to wait before applying the regularization, in  $[0, 5000, 10000, 15000, 20000]$ .

For each regularization schema, we select the model with the best binary validation accuracy, and the corresponding results are displayed in Table 1. Detailed hyperparameter configurations are provided in Table 2 for reference.

We investigate the effects of each hyperparameter.

**Bias Reparametrization** For the choice of bias reparametrization function, we observed that not applying any reparametrization to the bias resulted in less robustness, and the network occasionally failed to learn. Applying projected reparametrization improved robustness, but it did not increase the proportion of activated neurons. Conversely, applying the positive projected and projected reparametrization functions increased the ratio of activated BiSE neurons from 0.9% to around 20%. Ensuring that the bias falls within the correct range of values enhances the interpretability of the network.

**Regularization Delay** when activating the regularization loss at the beginning of training, the results were notably worse, especially in binary accuracy. Our hypothesis is that the network does not have enough time to explore the right morphological operations and is prematurely drawn to a non-optimal operator, getting stuck in its vicinity. We observed that the accuracy improved when increasing the waiting time before activating the regularization loss. Future work may explore more advanced policies for applying the loss, such as using the loss at a given frequency instead of every batch, increasing the coefficient of the loss at each step, or waiting for the network to converge before applying regularization.

**Regularization coefficient and last activation** The coefficient of the regularization loss did not have a significant impact, as well as replacing the normalized tanh by a softmax layer.